

Improving Electrochemical Performance of (Cu, Sm)CeO₂ Anode with Anchored Cu Nanoparticles for Direct Utilization of Natural Gas in Solid Oxide Fuel Cells

Zhicheng Wang, Yang Wang, Delong Qin, Yiheng Gu, Hailin Yu, Shi Tao, Bin Qian, Yimin Chao



PII: S0955-2219(22)00098-X

DOI: <https://doi.org/10.1016/j.jeurceramsoc.2022.02.006>

Reference: JECS14651

To appear in: *Journal of the European Ceramic Society*

Received date: 3 September 2021

Revised date: 26 January 2022

Accepted date: 2 February 2022

Please cite this article as: Zhicheng Wang, Yang Wang, Delong Qin, Yiheng Gu, Hailin Yu, Shi Tao, Bin Qian and Yimin Chao, Improving Electrochemical Performance of (Cu, Sm)CeO₂ Anode with Anchored Cu Nanoparticles for Direct Utilization of Natural Gas in Solid Oxide Fuel Cells, *Journal of the European Ceramic Society*, (2021)
doi:<https://doi.org/10.1016/j.jeurceramsoc.2022.02.006>

This is a PDF file of an article that has undergone enhancements after acceptance, such as the addition of a cover page and metadata, and formatting for readability, but it is not yet the definitive version of record. This version will undergo additional copyediting, typesetting and review before it is published in its final form, but we are providing this version to give early visibility of the article. Please note that, during the production process, errors may be discovered which could affect the content, and all legal disclaimers that apply to the journal pertain.

© 2021 Published by Elsevier.

Improving Electrochemical Performance of (Cu, Sm)CeO₂ Anode with Anchored Cu Nanoparticles for Direct Utilization of Natural Gas in Solid Oxide Fuel Cells

Zhicheng Wang^{a,*}, Yang Wang^a, Delong Qin^a, Yiheng Gu^a, Hailin Yu^a, Shi Tao^a, Bin Qian^{a,*}, Yimin Chao^{b,**}

^aSchool of Electronic and Information Engineering, Changshu Institute of Technology, Changshu 215500, PR China

^bSchool of Chemistry, University of East Anglia, Norwich NR4 7TJ, UK

Abstract

Development of solid oxide fuel cell (SOFC) anode with high resistance to coking and sulfur poisoning is highly desirable for the direct application of natural gas in SOFC. Herein, a (Cu, Sm)CeO₂ anode with anchored Cu nanoparticles has been prepared. Most of Cu nanoparticles particle size ranges from 20 to 50 nm, which can increase the conductivity and catalytic activity of the anode. The Cu/CSCO10 supported cell exhibits a maximum power density of 404.6 mW/cm² at 600 °C when dry methane is used as fuel while its ohmic resistance is only 0.39 Ω·cm². The single SOFC shows good stability when H₂S content in the fuel is less than 150 ppm. Up to 900 hours of continuous stable operation with simulated natural gas and commercial natural gas as fuel prove the advantages and application potential of this anode.

Keywords: solid oxide fuel cell, copper nanoparticles, coking-resistant, sulfur tolerance, natural gas

1. Introduction

Natural gas is a clean and environmentally friendly high-quality energy [1-3], in comparison with other fossil cells. With the development of the exploitation technology of unconventional natural gas, such as shale gas [4-6] and hydrated natural

* Corresponding author. Fax: +86 512 52251552. E-mail address: wangzc@csig.edu.cn, wzc877@zju.edu.cn (Z. Wang)

* Corresponding author. Fax: +86 512 52251170. E-mail address: njqb@csig.edu.cn (B. Qian)

** Corresponding co-author. Tel.: +44 1603 59 3146; Fax: +44 1603 59 2003. E-mail address: Y.Chao@uea.ac.uk (Y. Chao)

gas [7-8], the proportion of methane dominated natural gas in the world energy consumption is increasing [9]. According to BP Statistical Review of World Energy 2021, the share of gas in primary energy continued to rise, reaching a record high of 24.7% in 2020 [10]. SOFCs can directly use natural gas as fuel in principle [11-13], which can not only improve the utilization efficiency of natural gas, but also avoid the resource shortage and environmental pollution, so as to achieve the goal of sustainable development [14, 15]. However, when commercial natural gas is directly used as fuel, SOFC could suffer the problems of carbon deposition and sulfur poisoning, which can deactivate catalysts by covering or poisoning the active sites of the anode and thus inhibit reactions [16-18].

Ceria (cerium oxide) is a well-known oxidation catalyst [19] which is expected to increase the activity of the anode for the electrochemical oxidation of hydrocarbon [20-22]. Doping ceria has been the subject of great interest because the addition of dopants greatly increases the concentration of oxygen vacancies, enhances catalytic activity of hydrocarbon oxidation and improves thermal stability of ceria [23, 24]. Rare earth oxides with trivalent cations, such as Sm^{3+} and Gd^{3+} [25-27], are the best possible dopants for modifying structural and chemical properties of ceria because these elements can easily replace cerium on its regular sites. Moreover, a rich number of oxygen vacancies in the doped ceria lattice increase the mobility of oxygen ions that enables the oxygen anions to interact with H_2S at the running temperature of SOFCs. This results in the oxidation of H_2S to sulfur oxides, which are much more easily removed and thus prevents sulfur poisoning [28]. As a mixed ionic/electronic conductor (MIEC), doped ceria allows simultaneous transport of both ionic and electronic defects [29-31], but the electronic conductivity of doped ceria fails to meet the requirements of SOFC when it is directly used as anode material [32].

By incorporating anti-coking and sulfur-resistant metals into doped ceria to form the anode, the operating lifetime and performance of the SOFC can be enhanced with natural gas as fuel. Compared with noble metals [33, 34], which have strong catalytic activity and sulfur tolerance, Cu catalyst has been employed to enhance sulfur tolerance and inhibit carbon deposition due to its low cost and high catalytic activity

[34-36]. Meanwhile, the electrochemical activity and sulfur resistance of the anode containing copper can be enhanced by the synergistic effect generated by the interaction of copper with doped ceria [37]. It has been proved that the Cu-ceria based anodes with nanostructure can obtain reasonable power density when using hydrocarbon as fuel and has good resistance to coking and sulfur poisoning.

At present, Cu-ceria anodes are mainly fabricated by wet impregnation method [38, 39]. The Cu precursor solution is impregnated into pre-sintered highly porous Sm-doped ceria (SDC) framework on the dense electrolyte and the loaded copper oxides are subsequent reduced to form nano-sized copper particles adhering on the surface of SDC. However, the copper particles tend to agglomeration and grain growth at operation temperature of SOFCs [40]. Recently, No Woo Kwak *et al* [41] have proposed an *in situ* synthesis of supported metal nanocatalysts through heterogeneous doping. The whole preparation process includes metal source coating, heterogeneous doping, metal source etching and reduction. Uniformly distributed copper nanoparticles (NPs) are synthesized via heterogeneous doping of copper cations along the grain boundaries of SDC and then to reduce the diffused copper cations to form nanoclusters. The resulted Cu NPs are mainly located at junctions where SDC grain boundaries meet and hold strong anchorage with the oxide surface, which can effectively suppress the growth of metallic particles and show high chemical durability with excellent electro-chemical catalytic activity. The processes of the afore-mentioned two methods are too complicated to be applied in large-scale preparation of SOFCs.

As an one-step environmentally friendly method, *in situ* exsolution provides an attractive route for the preparation of SOFCs because it can produce coking-resistant and socketed metal particles in anode and tailor particle-substrate interactions [42-44]. In this work, copper and samarium co-doped ceria (CSCO) is used as anode precursor material to produce the (Cu, Sm)CeO₂ anode with anchored Cu nanoparticles. The catalytic activity and conductivity of ceria are improved by ion doping and exsolution. The performance and stability of the single SOFC are investigated with natural gas as fuel. The formation mechanism of anode and the mechanism of anti-coking and sulfur

poisoning resistance are exploited by structural analysis and static electronic structure calculations.

2. Experimental methods

2.1. Electrodes and electrolyte materials preparation

Powder of CSCO was synthesized by the glycine-nitrate combustion method. The stoichiometric amounts of cerium nitrate, samarium nitrate and copper nitrate were dissolved into deionized water. Then the glycine were added into the solution with the total molar ratio of $M_{\text{NO}_3^-}:M_{\text{glycine}} = 2:1$, and the solution was heated and stirred at 80 °C until glycine was completely dissolved. Afterwards, the resultant solution was heated on an electric tabletop burner until it was ignited to produce a sponge-like metal-oxide ash. The ash was subsequently kept for 2h at 700 °C in a furnace to remove possible carbon residues and a well-crystalline oxide powder was obtained. In this work, the molar ratio of Ce^{4+} to Sm^{3+} was always controlled at 4:1 in CSCO powder, while the mole doping amount of Cu starts from 5% and increases gradually with 2.5% step.

Powders of SDC and SSC ($\text{Sm}_{0.5}\text{Sr}_{0.5}\text{CoO}_3$) were also prepared with the same method, and $\text{Ce}(\text{NH}_4)_2(\text{NO}_3)_6$ with 25% mole ratio was added as cerium ion source when SDC powders were prepared to reduce the sintering temperature of SDC electrolyte [45].

The 70 wt.% SSC powder and 30 wt.% SDC powder were mixed by wet ball-milling for 72h in ethanol to form the cathode material. The as-prepared SDC were also milled in ethanol in a planetary ball-milling and then dried at 50 °C.

2.2. Single fuel cell manufacture

The anode-supported cells were fabricated with the configuration Cu/CSCO_x (~500 μm) | SDC (~30 μm) | SSC/SDC (~30 μm), where the value of *x* is determined by the mole doping percentage of Cu. CSCO powders were mixed with polystyrene (15 wt.%, foaming agent) in ethanol in an ultrasonic bath and dried at 50 °C. Cylindrical pellets of 15 mm diameter and ~1mm thickness were prepared by uniaxial pressing at 100 MPa. Then, the SDC powders were co-pressed on the one side of pellet at 200 MPa as the electrolyte layer. The pellets were co-sintered at 1250 ± 5 °C for 5 h in a furnace (Nabertherm, Germany). The cathode layer was prepared by a spin-coating method. The cathode suspension was made by ultrasonically dispersing a mixture of 90 wt.% cathode material and 10 wt.% ethylcellulose in ethanol while the volume ratio of liquid/solid was kept at 10. The suspension was spin-coated onto the electrolyte surface and subsequently sintered at 950 °C for 2 h to form a porous cathode. The sintered pellet was reduced in the flowing H₂ at 700 °C for 4 h to obtain the single cell.

2.3. Structural characterization and theoretical calculation

The crystalline phase of the anode precursor powders was analyzed by X-ray diffraction (XRD, Bruker) with Cu K_α radiation. The morphology and microstructure of the anode powders were investigated by transmission electron microscope (TEM, JEM-2000CX, JEOL) and high-resolution TEM (HRTEM). The elemental constitution of the anode powders was characterized by energy dispersive spectroscopy (EDS).

The crystallographic information of the anode was also characterized by XRD. The chemical composition and state on the surface of the anode were studied by X-ray photoelectron spectroscopy (XPS, PHI-5400, PE) with an Al K_{α} source, and the data were analyzed using Casa XPS software. The spectra were calibrated based on the C $1s$ peak from adventitious carbon. Quantification was performed based on the area of peaks of interest (Cu $2p_{3/2}$, O $1s$) after a linear background subtraction. The cross-sectional morphological and microstructural details of the anode were examined with scanning electron microscope (SEM) and element mapping (SIGMA, ZEISS). The outlet gas composition of the anode was analysed by a Fourier-transformed Infrared Spectroscopy (FTIR, Spectrum 100, PerkinElmer) when dry methane was directly fueled to the single SOFC. The proportion of different carbonaceous gases was calculated according to the concentrations of CH_4 , CO_2 and CO after the calibration process [46].

The geometry structure relaxations and static electronic structure calculations are performed by using the VASP package [47, 48]. The generalized-gradient approximation (GGA) of Perdew–Burke–Ernzerhof (PBE) [49] and projector augmented wave (PAW) potentials are used. The cutoff energy is set to be 600 eV and a $7 \times 7 \times 7$ Monkhorst-Pack k-points grid is used. All of the geometry structures are fully relaxed until forces are converged to 0.01 eV/\AA .

2.4. Electrochemical characterization

Electrochemical analysis of all cells was carried out using a CHI760C Electrochemical Workstation (CH Instrument, China) in a two-electrode configuration.

Silver paste was used to seal the anode compartment onto a quartz tube. Current collectors (0.003 in Ag-mesh, Alfa Aesar) were sintered onto both electrodes and two silver wires (Alfa Aesar, 0.01 in) were used as the leads (Figure S1, Supporting Information). AC amplitude of 10 mV was used. The measurement frequency range was from 0.01 Hz to 100 kHz. The polarization curves (I-V curves) were generated using the Linear Sweep Voltammetry feature in the Electrochemical Workstation software package, sweeping from the measured open circuit voltages (OCVs) to 0 V with a scan rate of 20mV and 1 mV step size. All cells were placed inside a quartz tube into which the different fuels were delivered via digital volumetric flowmeter. The fuel flow rate was fixed at 60 ml/min while the cathode was placed in the atmosphere. The methane, H₂S-contaminated methane, simulated natural gas (SNG) and NG were used as fuel to verify the catalytic performance and stability of single cell in this work.

3. Results and discussion

3.1 Material characterization of powders

The crystalline structure of Ce_{0.72}Sm_{0.18}Cu_{0.1}O_x is revealed by XRD measurement. As shown in Fig. 1a, all the diffraction peaks are in good agreement with the JCPDS standard (card no. 43-1002), corresponding to fluorite structured face-centered cubic CeO₂ phase. Notably, there are no additional peaks of CuO and Sm₂O₃ being detected, suggesting the pure Ce_{0.72}Sm_{0.18}Cu_{0.1}O_x has been synthesized. As shown in Fig. 1b, high-resolution TEM image reveals a crystalline individual nanoparticle, which has clear lattice fringes with an interplanar spacing of 0.314 nm. This can be readily

assigned to the d spacing of (111) plane of the CeO_2 . Additionally, the elemental mappings of Cu, Sm, Ce, and O demonstrate that they are uniformly dispersed in the sample, revealing the single phase of the sample (Fig. 2c, d). However, when the doping amount of Cu reaches 12.5%, CuO phase could be formed in the powder (Figure S2, Supporting Information).

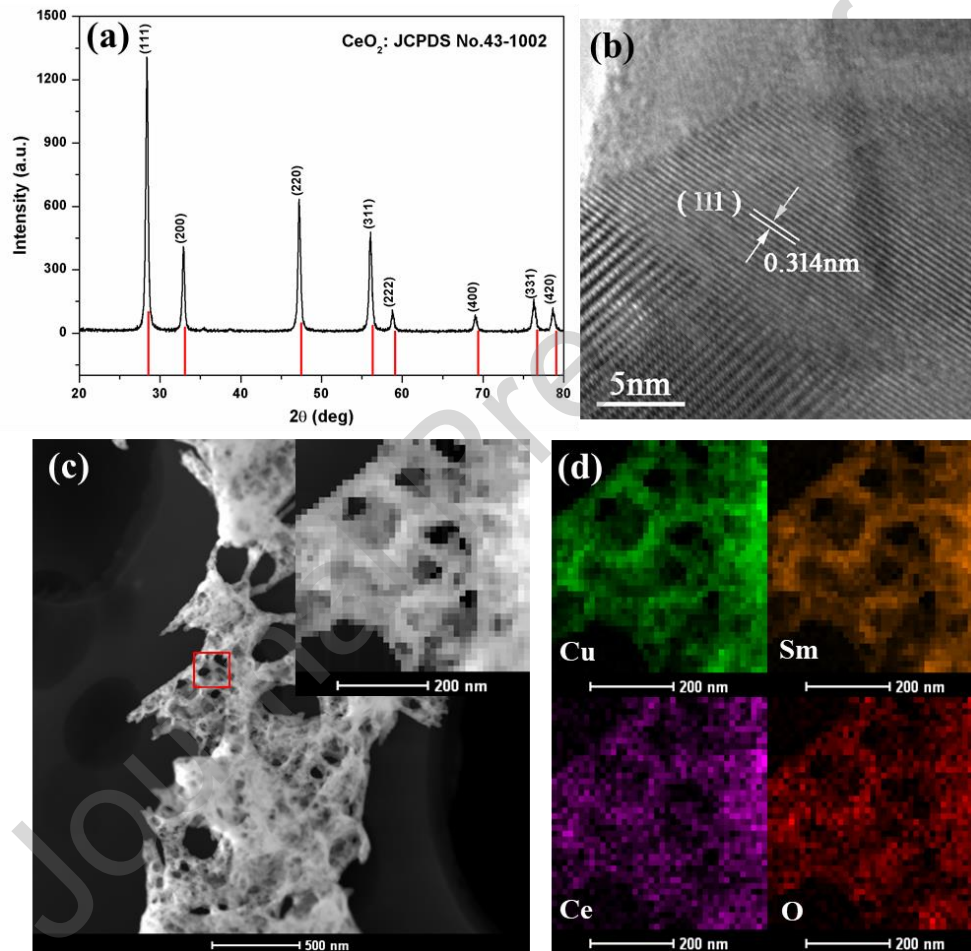


Figure 1. Characterizations of the $\text{Ce}_{0.72}\text{Sm}_{0.18}\text{Cu}_{0.1}\text{O}_x$ powders. (a) XRD pattern. (b) high-resolution TEM image. (c,d) STEM image and corresponding elemental mapping

3.2 Microstructure and formation of anode

In this work, three different anode-supported cells were prepared by using $\text{Ce}_{0.76}\text{Sm}_{0.19}\text{Cu}_{0.05}\text{O}_x$, $\text{Ce}_{0.74}\text{Sm}_{0.185}\text{Cu}_{0.075}\text{O}_x$ and $\text{Ce}_{0.72}\text{Sm}_{0.18}\text{Cu}_{0.1}\text{O}_x$ powder as anode precursors and labeled as Cu/CSCO5, Cu/CSCO7.5 and 10Cu/CSCO10 supported cell

respectively.

Fig. 2a is a schematic procedure of preparing a novel Cu/CSCO_x anode, it can be seen that the anodic porous frame is composed of lower copper-doped CSCO (L-CSCO) when parts of the CuO is converted into copper NPs anchoring on its surface after the exsolution procedures, which demonstrates the redox exsolution method can effectively produce the Cu/CSCO_x anodes. The crystalline structure of the samples at different preparation stages are revealed by XRD measurement. As shown in Fig. 2b, the anode ceramic before reduction contains two phases of CSCO and CuO, indicating that when CSCO powder is sintered into porous ceramic, a small amount of CuO has been separated from CSCO crystal at the grain boundaries. According to the lattice parameters of L-CSCO obtained by calculating XRD data through cell refinement function in the Jade6.5 software, it can be estimated [50] that the mole percent of Cu²⁺ remaining in the crystal structure of CSCO5 anode, CSCO7.5 anode and CSCO10 anode are 1.41%, 1.79% and 2.28%, respectively (see more data in Table S1, Supporting Information), which is close to the mole percent of Cu²⁺ remaining in the crystal structure obtained from the XPS data.

Fig. 2c shows the cross-sectional microstructures of the porous anode ceramics before reduction, the ceramic surface is relatively smooth, and the grains on the anode ceramic skeleton are closely linked, forming a continuous porous three-dimensional structure. Fig. 2d shows the cross-sectional microstructures of the porous anode ceramics after reduction, it can be seen that Cu particles were formed in the framework of different porous anode (see more data in Figure S3, Supporting

Information). From the further enlarged SEM image and corresponding EDS mapping of the copper and oxygen distribution (Fig. 2e), it can be seen that a large number of Cu NPs are clearly exuded from the crystal and anchored on the surface of the porous ceramic frame, which can effectively prevent the agglomeration of Cu NPs [42]. Meanwhile, some large size Cu particles appear on the grain boundary of L-CSCO.

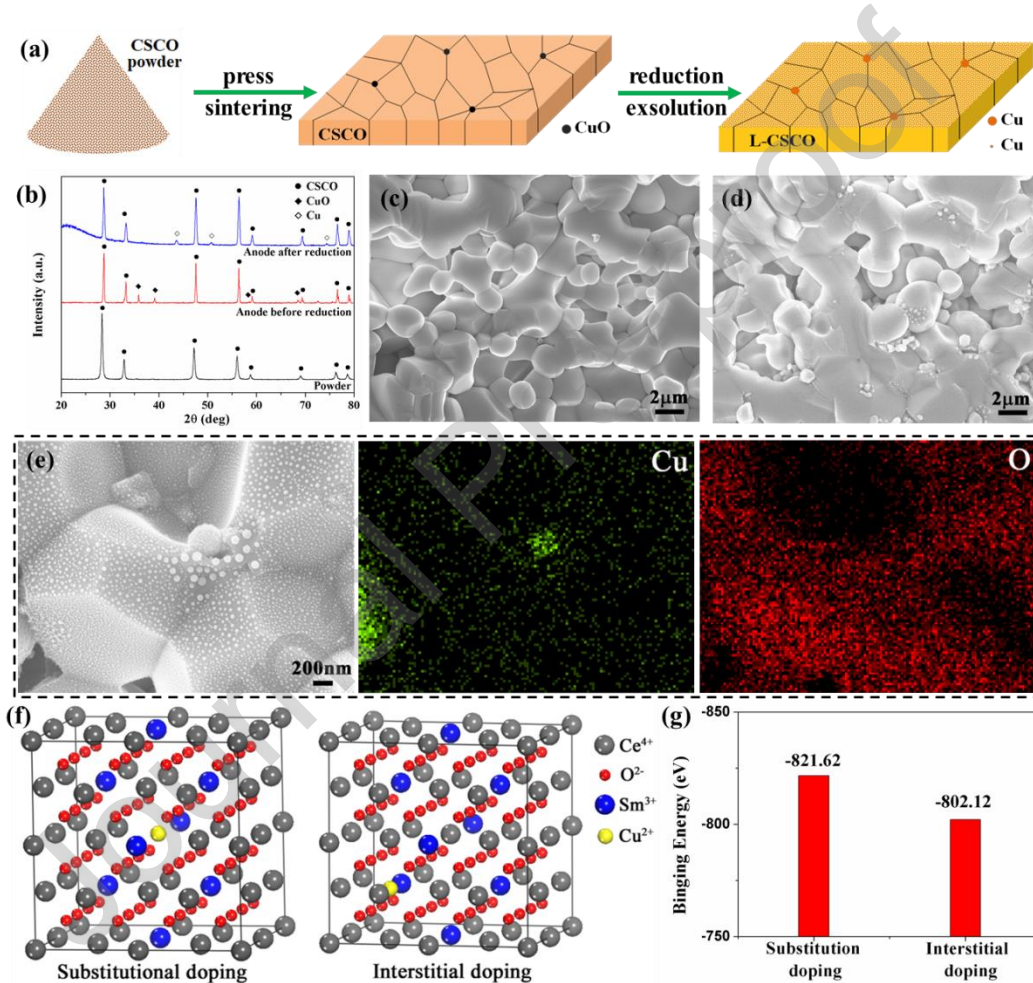


Figure 2. (a) Schematic illustration of the synthesis route for $x\text{Cu}/\text{SDC}$ anode. (b) XRD patterns of CSCO powder and anode before and after reduction. (c, d) Cross-sectional SEM image of the porous anode ceramics before and after reduction. (e) High-resolution SEM image of the anode and corresponding EDS mapping of the copper and oxygen distribution of anode. (f) The geometric configurations of CSCO crystal structure. (g) The calculated binding energy of copper ion in different geometric configurations.

This phenomenon is mainly determined by the position of copper ion in solid

solution. As shown in Fig. 2f, both substitution doping and interstitial doping can be formed because the radius of the Cu^{2+} (73 pm) is smaller than that of Ce^{4+} (97 pm) and Sm^{3+} (107.9 pm) [51-53]. Due to the different position of Cu in the crystal, the binding energy between copper ion and other ions is also different. The simulation results show that the binding energy is -821.62 eV when the copper ion is at substitution position and it is -802.12 eV when the copper ion is at interstitial position shown in Fig. 2g. Therefore, the copper ions enter the substitution sites first in the doping process, and the corresponding CSCO (111) diffraction peak shifts to the lower angle due to the smaller radius of copper ion. With the increase of copper ion doping content, the copper ions will enter the interstitial sites and the lattice parameter also increases, which lead to the diffraction peak moves to the higher angle.

The calculated binding energy suggests that the binding energy of substitutional copper ions are much stronger than that of interstitial copper ions. Compared with the substitutional copper ions, the interstitial copper ions are more easily dissolved, so some CuO exuding from the crystal during the sintering process, gathering on the grain boundary, and then forming larger particles of Cu after reduction, and another part of Cu elements exuding from the crystal during the reduction process, and evenly distributed on the L-CSCO crystal surface. The formation of Cu can enhance the conductivity of the anode. Meanwhile, it can increase the specific surface area and the triple phase (gas phase, ion phase, electronic phase) boundaries (TPBs) of the anode, which is conducive to the rapid adsorption of gas and the occurrence of more catalytic reactions. Cu NPs anchored on CSCO would increase the catalytic activity for the

hydrocarbon and deliver enhanced synergistic effect on coking resistance during hydrocarbon oxidation in the anode [54, 55].

Fig. 3 shows the distribution of Cu NPs on the porous ceramic frame surface of different cells. It can be seen that most of Cu NPs particle size ranges from 20 to 50 nm. In addition, the distribution density of copper NPs increases with the increase of copper doping, which helps to provide more TPBs for hydrocarbon oxidation.

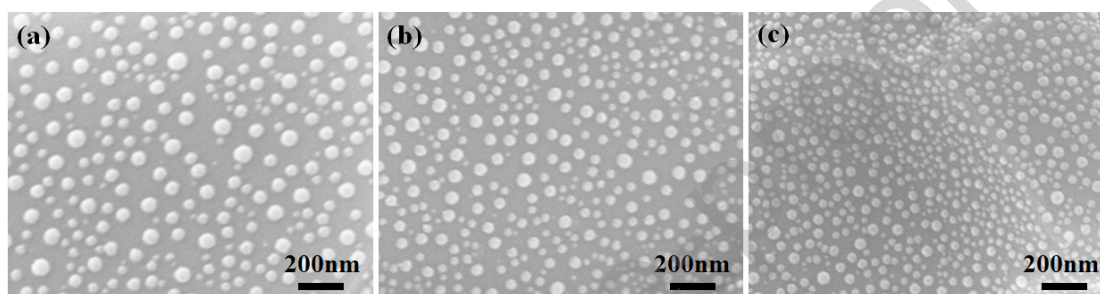


Figure 3. SEM images of the distribution of Cu NPs on the porous ceramic frame surface: (a) Cu/CSCO5, (b) Cu/CSCO7.5 and (c) Cu/CSCO10.

3.3 Electrochemical performance

In order to investigate the performance of the cells with different anodes for direct oxidation of Hydrocarbon, dry methane was directly fueled to the single SOFCs at 600 °C. Fig. 4a shows the voltage and power density as a function of current density for three different anode-supported cells, where the OCVs of Cu/CSCO5, Cu/CSCO7.5 and Cu/CSCO10 supported cells are 0.987, 0.950 and 0.931 V, respectively. These results are close to or greater than the theoretical value for methane complete oxidation, which indicates that complex reactions have taken place in the anode at initial stage. As shown in Figure S5, both CO₂ and CO was produced in the outlet gas and the CO₂ yield increased when reactions were carried out for 100h. These results indicate that in addition to the complete oxidation (reaction 1) and

partial oxidation of methane (reaction 2), there are also oxidation reactions of CO (reaction 3) and H₂ (reaction 4) taking place under the synergistic catalysis of Cu and SDC. The maximum power densities for Cu/CSCO5, Cu/CSCO7.5 and Cu/CSCO10 supported cells are 249.6, 338.9 and 404.6 mW/cm², respectively. The results show that high performances are achieved based on the Cu/CSCO_x anode and the cell performance increases with the increase of Cu content in the Cu/CSCO_x anode at the same testing temperature. This is mainly due to the increase of copper content, which can generate more Cu NPs in the anode and anchor on the L-CSCO framework, enhancing the synergistic effect of Cu and L-CSCO by providing more effective reaction sites for electrochemical reaction.

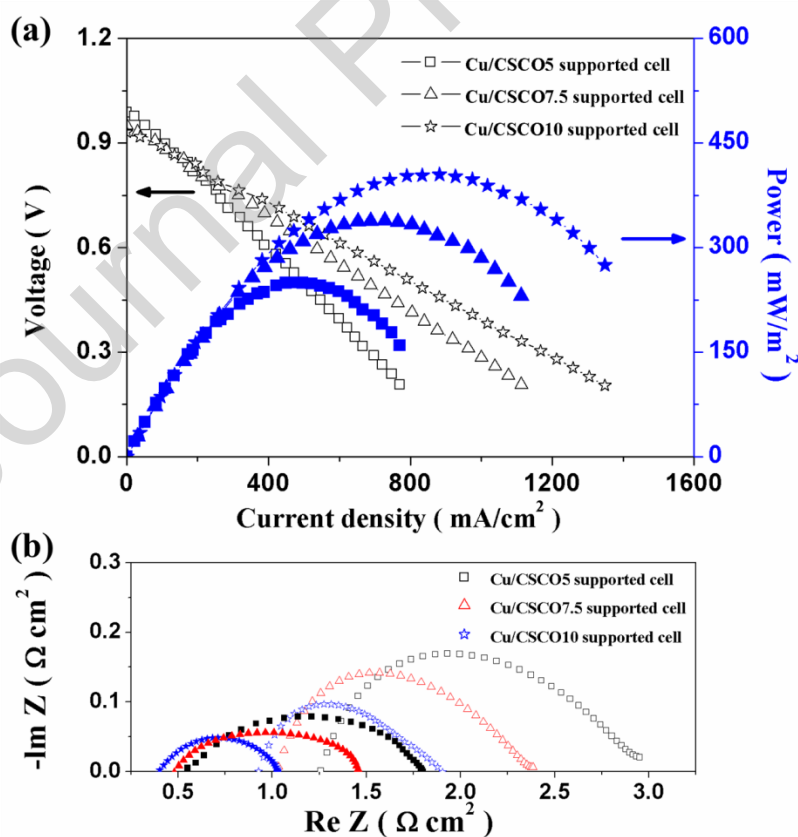
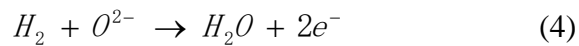
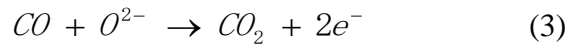
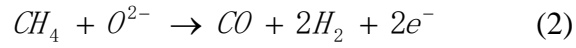
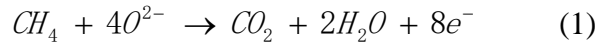


Figure 4. (a) Cell voltages (open symbols) and power densities (solid symbols) as function of current density of different anode supported cells tested at 600 °C with dry CH₄ as fuel. (b) Impedance spectra measured at 600 °C under open circuit conditions

for different anode supported cells before (open symbols) and after (solid symbols) running with dry CH₄ as fuel.



The polarization resistance of electrodes and the inherent ohmic resistance of the cells were measured by electrochemical impedance spectra (EIS) at 600 °C under open circuit conditions. Fig. 4b shows the typical EIS Nyquist plots of different cells before and after running with dry CH₄ as fuel. The ohmic resistance corresponds to the intercept of the EIS Nyquist plot at high frequency on the left and the polarization resistance of electrodes corresponds to the intercepts on the real axis between high and low frequency. It can be seen from Fig. 4b that the ohmic resistance of Cu/CSCO5, Cu/CSCO7.5 and Cu/CSCO10 supported cells decrease from 1.24, 1.01 and 0.90 Ω·cm² before reduction to 0.54, 0.49, 0.39 Ω·cm² after reduction respectively. These results are close to the ohm resistance of our previous single SOFC supported by Ni-SDC anode [37] or Cu-GDC anode prepared by sintered [56] that indicates copper doping and the formation of Cu NPs can reduce the ohmic resistance of the anode. The substantial improvement of anode conductivity could be attributed to that: (1) with the increase of copper content in the anode, the density of the exsolved Cu NPs increases as shown in Fig. 3, this will provide more channels for electron transmission in the anode due to the formation of a thin and continuous

network on the surface of the porous scaffold [39], the theoretical research showed that as long as a 5.8 vol% Cu loading could produce a 1460 S/cm conductivity with an ideal conformal coating in the anode [57], and *in situ* exsolution is one of the most likely preparation method to realize such microstructure in porous structure; (2) as the favorable sites for heterogeneous nucleation, the grain boundaries allow metal particles to be ex-solved readily at relatively low temperatures [41], so some Cu NPs gather along the grain boundaries of host oxides to form a continuous network for electron transmission; (3) the residual of a small amount of Cu in SDC crystal is conducive to improve the conductivity of SDC itself, the research [58] showed that doping 1% copper can increase the conductivity of $\text{Ce}_{0.8}\text{Gd}_{0.2}\text{O}_{2-\delta}$ by 4 times at 600 °C, the mole percent of Cu^{2+} remaining in the crystal structure of CSCO10 anode has reached 2.28%; (4) the single cell in this work was sealed with silver paste, which is also benefit for the collection of anode current.

Fig. 4b also shows the effect of doping amount of copper on the SOFC performance. It can be seen that the polarization resistance decrease significantly with increase of the doping amount of copper. Furthermore, the polarization resistance values of Cu/CSCO5, Cu/CSCO7.5 and Cu/CSCO10 supported cells are 1.25, 0.94 and $0.61 \text{ } \Omega \cdot \text{cm}^2$ after running, which decreases by 28.6%, 31.4% and 35.8% compared with that before reduction respectively (Table S2, Supporting Information). The conductivity and catalytic activity of anode is apparently improved by the increase of doping amount of copper after reduction.

Comparing with other Cu-based-anode structures prepared by impregnation

methods [57, 59], the performance of the single cell in this work has been greatly improved. It is well known that ionic conductivity is also one of the crucial parameters of the anode at low temperature besides catalytic activity and electrical conductivity. The Cu-based-anodes prepared by impregnation method often use YSZ (yttria-stabilized zirconia) scaffold as the porous anode substrate and the oxygen ions in the electrode are conducted to TPBs through YSZ scaffold. The ionic conductivity of YSZ at low temperature is 1~ 2 orders of magnitude lower than that of SDC [60]. Furthermore, a small amount of Cu^{2+} remaining in the SDC crystal can enhance the grain boundary ionic conductivity [61]. Therefore, L-CSCO can provide more oxygen ions for TPBS for fuel oxidation reaction to improve cell performance. In addition, different from the exsolution method, the impregnation method is difficult to make the reaction activation points evenly distributed in the whole porous anode, and even block some pores, affect the transmission of fuel gas and reduce the utilization rate of anode.

3.4 Long term stability

The coking resistance of the anode has been studied in Cu/CSCO10 supported cell. As shown in Fig. 5, the current density at 0.5 V is very stable for 300 hours with dry CH_4 as fuel. The sensitivity of this anode to the sulfur poisoning has been investigated by gradually increasing the concentration of H_2S in methane. In Fig. 5, the current densities at 0.5V of the same cell are plotted as a function of time with different concentrations of H_2S in methane at 600 °C. There is no observable change in current density as the fuel switched from clean methane to methane contaminated

with 50, 100 or 150 ppm H₂S. With fuel methane containing 200 ppm H₂S, the power output of the cell is slightly dropped. The SOFC performance degradation is mainly due to the formation of ceria-sulfur compounds [62, 63] because ceria is more sensitive to sulfur than Cu.

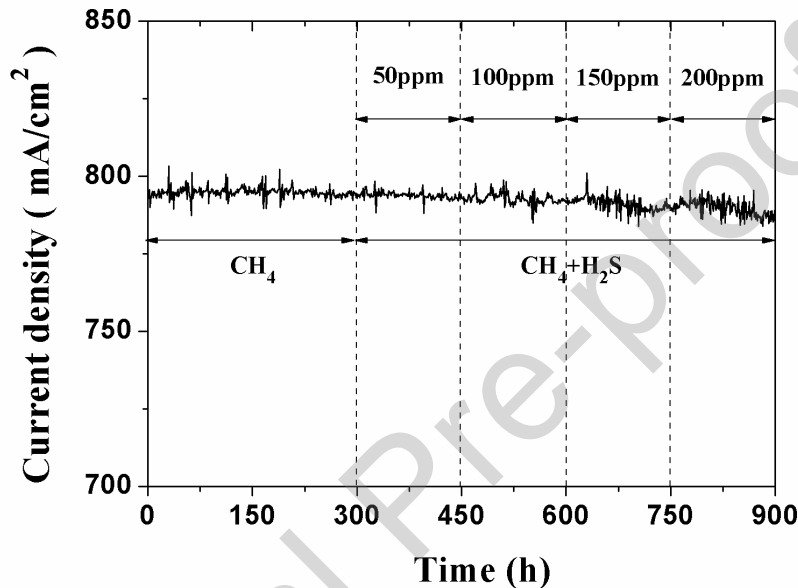


Figure 5. Current density of Cu/CSCO10 supported cell operated at 600 °C with a constant cell voltage of 0.5 V as the fuel was switched from dry CH₄ to CH₄ contaminated with different concentrations of H₂S.

Continuous and stable operation in dry methane for 300 hours without observable degradation in performance suggests that this type of anode is very effective for directly oxidizing methane and inhibiting coking. Moreover, there is no observable change in power output for 150 hours when the fuel is switched to methane contaminated with 150 ppm H₂S. Continuous and stable operation in H₂S-contaminated methane for a longer period of time (300 to 750 hours) confirms that sulfur poisoning can be fully suppressed in the anode when H₂S content in the fuel is less than 150 ppm. All these results show that the anode has good resistance to

carbon deposition and sulfur poisoning, and can be directly used for direct oxidation of natural gas.

3.5 Catalytic mechanisms of inhibiting coking and enhancing sulfur tolerance

When SOFC directly uses methane or methane based natural gas as fuel, complete oxidation and partial oxidation of methane may occur on the anode. When methane is completely oxidized by oxygen ions to generate CO_2 and H_2O , electrons are released. While methane is partially oxidized by oxygen ions, CO and H_2 are generated, and the generated CO and H_2 are to be oxidized further under the action of catalyst. If CO is not oxidized by catalysis, the concentration of CO is to be increased gradually, resulting in carbon deposition cumulated on the anode, which is a problem with traditional anode materials. Although the catalytic oxidation activity of copper in the anode to hydrocarbon is low, the catalytic activity for the oxidation of CO is higher [64]. Therefore, it is possible to inhibit coking on the surface of the Cu/CSCO_x anodes.

High-resolution XPS measurements have been employed in order to further examine the surface composition and the chemical state of copper presented in the anode at different stages. As shown in Fig. 6a, a broad $\text{Cu } 2p_{3/2}$ peak and a shake-up peak (From 937 eV to 948 eV) are observed in the $\text{Cu } 2p$ spectra of the anode before reduction. The broad $\text{Cu } 2p_{3/2}$ signal can be fitted with two contributions at 933.1 eV and 934.8 eV by using the Gaussian fitting method with XPS peak software [52, 65]. The peak at higher $\text{Cu } 2p_{3/2}$ binding energy and the shake-up peak are two major XPS characteristic peaks of Cu^{2+} species, while the peak at lower $\text{Cu } 2p_{3/2}$ binding energy

is the characteristic peak of Cu^+ species. This result indicates that a small amount of Cu^+ is formed during the sintering process of CSCO ceramics, which also has been reported by other researchers [66]. After the reduction, a sharp characteristic peak appears at 932.1eV, the characteristic peak of Cu, which further proves the copper has exuded from the crystal and anchored on the surface of L-CSCO. Meanwhile, the intensity of the characteristic peak corresponding to copper ion is also enhanced, and with the operation of SOFC, the trend is more obvious (Table S3, Supporting Information). This is mainly due to the ability to store oxygen and the high oxygen ion conductivity of L-CSCO. After the formation of Cu particles, there are still copper oxides in the interface between Cu and L-CSCO, and more copper oxides will be formed at the interface when the oxygen ion O^{2-} is continuously transferred from the cathode to the anode through the oxygen vacancy of SDC during the operation of SOFC as shown in Fig. 6b (Figure S6, Supporting Information). Different valence states of Cu form a metastable copper cluster layer, which is composed of ion pairs such as $\text{Cu}^0\text{-Cu}^{2+}$, $\text{Cu}^+\text{-Cu}^{2+}$ and $\text{Cu}^+\text{-Cu}^0$ [57]. On the one hand, the metastable copper cluster layer has high electron conductivity to ensure the electron transfer in the electrode; on the other hand, it has strong redox ability, which makes it have high catalytic activity in the process of electrochemical reaction. The details of the mechanism of inhibiting carbon deposition by Cu/CSCOx anode are proposed as follows and are shown in Fig. 6c.

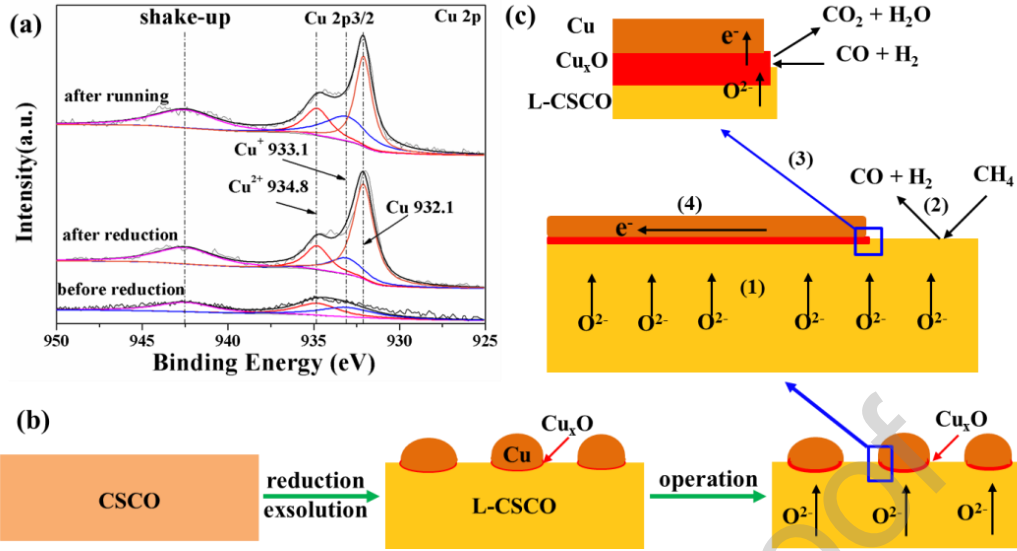
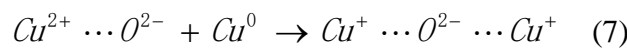
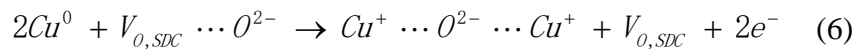
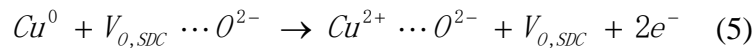


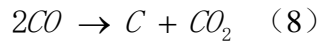
Figure 6. (a) XPS spectra of the Cu 2p in the Cu/CSCO10 anode at different stages. (b) Schematic representation of Cu-contained species at different stages. (c) Schematic representation of the synergistic catalysis of Cu and L-CSCO at the TPBs and the mechanism of inhibiting carbon deposition of Cu/CSCO_x anode.

Step (1): During the operation of a SOFC, the oxygen ions generated by the cathode are transferred to the anode through the oxygen vacancy of L-CSCO electrolyte. A series of oxidation reactions (reaction 5-7) occurred at the interface between Cu particles and SDC and the different valence states of Cu form a metastable copper cluster layer. Therefore, different from the traditional TPBs, in the TPBs of Cu/CSCO_x anode, L-CSCO plays the role of transmitting oxygen ions, Cu mainly plays the role of electron transfer, and the metastable copper cluster layer is the place of electrochemical reaction.



Step (2): L-CSCO in anode not only provides a path for oxygen ion transfer, but also catalyzes the oxidation of fuel. SDC in the anode mainly catalyzes incomplete

oxidation of methane. The generated CO will be disproportionated via the Boudouard reaction (reaction 8) and carbon deposition will occur at the anode. However, the metastable copper cluster layers are favorable for the adsorption of CO with single electron pairs and hydrogen.



Step (3): With the operation of SOFC, oxygen ions will be continuously transferred to the metastable clusters through the oxygen vacancies in SDC electrolyte, forming a shared oxygen ion with the adsorbed gas. The adsorbed CO is oxidized to CO₂ and desorbed, and electrons are produced. Thus, the CO concentration in the anode is effectively reduced and the carbon deposition is avoided. Similarly, H₂ is oxidized to H₂O and electrons.

Step (4): The generated electrons are conducted to the external circuit through Cu.

In conclusion, during the operation of the SOFC, the oxygen ion generated by the cathode is transferred to the anode through the oxygen vacancy of L-CSCO. At the interface between Cu and L-CSCO, part of Cu is oxidized to form the metastable copper cluster layer. Compared with the oxygen ion in the electrolyte vacancy, the oxygen ion in the metastable copper cluster layer is easier to lose, so it has higher oxidation property, which has great catalytic activity for the oxidation of CO and other gases generated during the operation of the SOFC, and generates a certain amount of electrons. Thus, carbon deposition is effectively inhibited.

Theoretical studies suggest that the presence of O²⁻ anions favors to suppress the

formation of the stable sulphides by converting the S-containing species into labile SO_2 [67]. The oxygen required for SO_2 formation can be derived from the lattice structures of the L-CSCO. Meanwhile, the metastable copper cluster layer in Cu/CSCO_x anode can enhance the catalytic activity for conversion of H_2S to SO_2 .

3.6 Performance with fueled natural gas

The SNG was prepared according to the Chinese national standard GB 17820-2018 [68], in which the molar composition includes 85% methane, 10% ethane and 5% propane. For comparison, 50 mg/m^3 (50 ppm) H_2S is added to SNG as fuel, where the additional amount of H_2S is higher than the control content of H_2S in commercial natural gas in the world (mostly 5 ppm-23 ppm) [69-71].

The performances of Cu/CSCO_{10} supported cell for direct oxidation of SNG and NG were tested (Figure S7, Supporting Information). The maximum power densities of Cu/CSCO_{10} supported cell fueled with SNG and NG are 420.3 and 415.2 mW/cm^2 at $600 \text{ }^\circ\text{C}$, respectively. It can be seen that the performance on SNG or NG exceeds that on pure methane. SNG or NG contains a small amount of linear alkanes, such as ethane and propane. The C-H bond strength of these alkanes decreases with the increase of hydrocarbon chain length, the oxidation and conversion of ethane and propane are easier than that of methane in the presence of appropriate catalysts [72]. Therefore, the performance has been improved when SNG or NG is used as fuels. As shown in Fig. 7, there is no observable change in current density when the fuel SNG is switched to one contaminated with 50 ppm H_2S for 600 hours. In the case of the commercial natural gas as fuel the performance of the cell remains steady during 300

hours of operation, although the output current density has dropped a little, this is mainly due to the difference of components between SNG and NG. In addition, at the same test voltage, the output current of single cell with SNG or NG as fuel is significantly higher than that with methane as fuel, indicating that the anode has good catalytic activity for the linear alkanes. These results show that the anode prepared in this paper is suitable for direct oxidation of commercial natural gas.

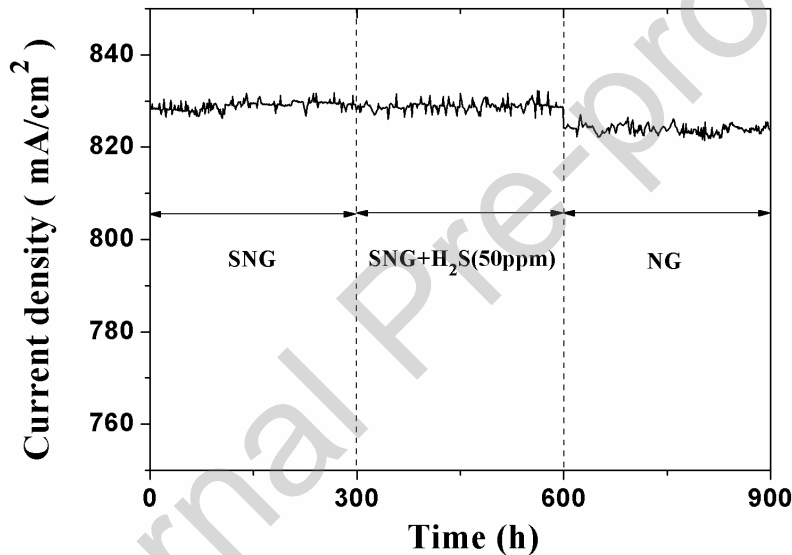


Figure 7. Current density of Cu/CSCO10 supported cell operated at 600 °C with a constant cell voltage of 0.5 V fueled with SNG, SNG+H₂S (50 ppm) and commercial NG.

The long-term operation stability benefits not only from the good resistance to coking and sulfur poisoning of the anode, but also from the stability of the anode microstructure. In Fig. 8, the SEM images of the cross-section of SOFC single cell after running with natural gas are shown. Fig. 8a shows cross-sectional microstructure and corresponding mapping of Ce, Cu and Co of the single cell. There are little changes in the morphology and no ionic migration observed after long running. The

microstructures of interface between cathode and electrolyte is shown in Fig. 8b, while interface between anode and electrolyte is shown in Fig. 8c. It can be seen that the dense SDC electrolyte layer is still strongly bonded to the porous electrodes and the electrodes retained their porous microstructure after cell tests. Furthermore, there is no obvious agglomeration of copper NPs after 900 hours running as shown in Figure S8. This result indicates that the microstructural features of the single cell still keeps stable after long running with natural gas.

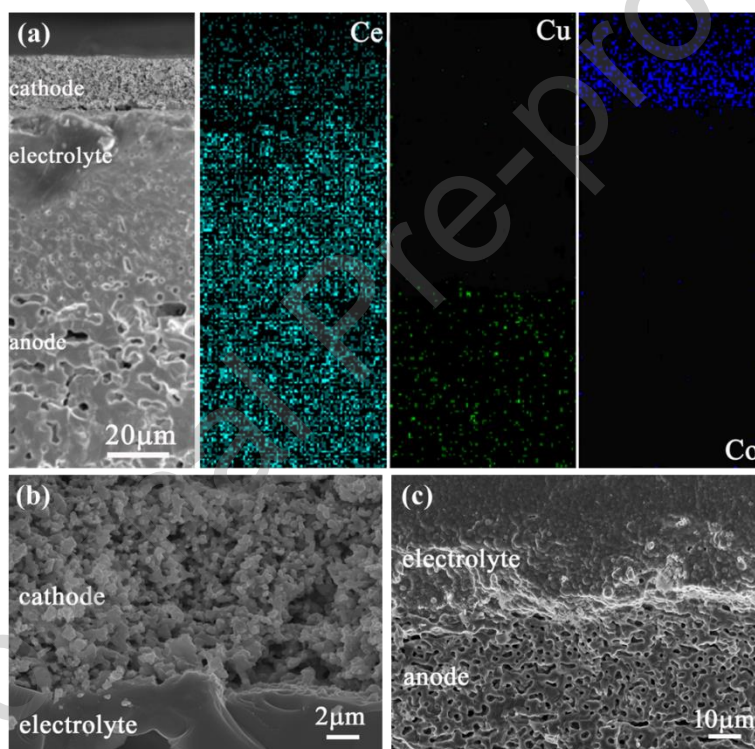


Figure 8. (a) SEM images of SOFC single cell cross-section and corresponding mapping of Ce, Cu and Co. (b) Microstructure of cathode/electrolyte interface. (c) Microstructure of anode/electrolyte interface.

4. Conclusions

In summary, an *in situ* exsolution with reduction method to fabricate the (Cu, Sm)CeO₂ anodes with anchored Cu nanoparticles for directly operating with natural gas has successfully developed. Up to 10 mol% Cu can be doped into SDC to form CSCo. Copper ions can enter into the substitutional site or interstitial site of ceria

lattice. The substitutional copper ions exclude from the crystal to form a large amount of Cu NPs after reduction and these Cu NPs anchor on the surface of the porous ceramic framework, most of Cu NPs particle size ranges from 20 to 50 nm, while the interstitial copper ions tend to dissolve during the sintering process because of the small binding energy and form a part of larger particles sitting on the grain boundary of the CSCO in the obtained Cu/CSCO_x anode. Electrochemical performance testing shows that the Cu/CSCO₁₀ anode possesses better conductivity and catalytic activity with dry methane as fuel. The corresponding cell exhibits a maximum power density of 404.6 mW/cm² at 600 °C while its ohmic resistance is only 0.39 Ω·cm². Continuous and stable operation in H₂S-contaminated methane confirm the strong ability to resist deactivation by carbon deposition and sulfur poisoning of the anode, because the catalytic activity for the hydrocarbon and sulfur oxidation has been enhanced by the metastable copper cluster. The maximum power density of 415.2 mW/cm² at 600 °C is achieved when natural gas is directly used as fuel. In addition, the long running cycles have proved that our single cell can directly use commercial natural gas as fuel.

Acknowledgments

This work was supported by the National Nature Science Foundation of China (11705015, U1832147); Suzhou Yuxin nanomaterial technology Co., Ltd. (KYH2020301Z) and Jiangsu student innovation and entrepreneurship training program (202010333015Z).

References

- [1] G. T. Chala, A. R. A. Aziz, F. Y. Hagos. Natural Gas Engine Technologies: Challenges and Energy Sustainability Issue. *Energies*, 2018, 11, 2934-2977. <https://doi.org/10.3390/en11112934>.
- [2] A. Burnham, J. Han, C. E. Clark, M. Wang, J. B. Dunn, I. Palou-Rivera. Life-Cycle Greenhouse Gas Emissions of Shale Gas, Natural Gas, Coal, and Petroleum. *Environ. Sci. Technol.*, 2012, 46(2), 619-627. <https://doi.org/10.1021/es201942m>.
- [3] M. A. M. Kinnon, J. Brouwer, S. Samuelsen. The role of natural gas and its infrastructure in mitigating greenhouse gas emissions, improving regional air quality, and renewable resource integration. *Prog. Energy Combust. Sci.*, 2018, 64, 62-92. <https://doi.org/10.1016/j.pecs.2017.10.002>.
- [4] Q. Wang, R. Li, Research status of shale gas: A review. *Renew. Sust. Energ. Rev.*, 2017, 74, 715-720. <https://doi.org/10.1016/j.rser.2017.03.007>.
- [5] Y. Yang, L. Wang, Y. Fang, C. Mou. Integrated value of shale gas development: A comparative analysis in the United States and China. *Renew. Sust. Energ. Rev.*, 2017, 76, 1465-1478. <https://doi.org/10.1016/j.rser.2016.11.174>.
- [6] Q. Wang, R. Li. Natural gas from shale formation: A research profile. *Renew. Sust. Energ. Rev.*, 2016, 57, 1-6. <https://doi.org/10.1016/j.rser.2015.12.093>.
- [7] B. R. C. Malagar, K. P. Lijith, D. N. Singh. Formation & dissociation of methane gas hydrates in sediments: A critical review. *J. Nat. Gas Sci. Eng.*, 2019, 65, 168-184. <https://doi.org/10.1016/j.jngse.2019.03.005>.
- [8] Y. Song, L. Yang, J. Zhao, W. Liu, M. Yang, Y. Li, Y. Liu, Q. Li. The status of natural gas hydrate research in China: A review. *Renew. Sust. Energ. Rev.*, 2014, 31, 778-791. <http://dx.doi.org/10.1016/j.rser.2013.12.025>.
- [9] B. B. Skabelund, H. Nakamura, T. Tezuka, K. Maruta, J. Ahn, R. J. Milcarek. Impact of low concentration hydrocarbons in natural gas on thermal partial oxidation in a micro-flow reactor for solid oxide fuel cell applications. *J. Power Sources*, 2020, 477, 229007. <https://doi.org/10.1016/j.jpowsour.2020.229007>.
- [10] BP p.l.c.. BP Statistical Review of World Energy 2021. 2021.
- [11] B. C. H. Steele. Running on natural gas. *Nature*, 1999, 400, 619-620. <https://doi.org/10.1038/23144>.
- [12] S. Park, J. M. Vohs, R. J. Gorte. Direct oxidation of hydrocarbons in a solid-oxide fuel cell. *Nature*, 2000, 404, 265-267. <https://doi.org/10.1038/35005040>.
- [13] S. McIntosh, R. J. Gorte. Direct Hydrocarbon Solid Oxide Fuel Cells. *Chem. Rev.*, 2004, 104, 4845-4865. <https://doi.org/10.1002/chin.200450267>.
- [14] Y. Bicer, F. Khalid. Life cycle environmental impact comparison of solid oxide fuel cells fueled by natural gas, hydrogen, ammonia and methanol for combined heat and power generation. *Int. J. Hydrog. Energy*, 2020, 45(5), 3670-3685. <https://doi.org/10.1016/j.ijhydene.2018.11.122>.
- [15] A. R. Shazed, H. M. Ashraf, M. A. Katebah, Z. Bouabidi, E. I. Al-musleh. Overcoming the energy and environmental issues of LNG plants by using solid oxide fuel cells. *Energy*, 2021, 218, 119510 1-15. <https://doi.org/10.1016/j.energy.2020.119510>.

- [16] A. Atkinson, S. Barnett, R. J. Gorte, J. T. S. Irvine, A. J. Mcevoy, M. Mogensen, S. C. Singhal, J. Vohs. Advanced anodes for high-temperature fuel cells. *Nat. Mater.*, 2004, 3, 17-27. <https://doi.org/10.1038/nmat1040>.
- [17] T. Y. Yeo, J. Ashok, S. Kawi. Recent developments in sulphur-resilient catalytic systems for syngas production. *Renew. Sust. Energ. Rev.*, 2019, 100, 52-70. <https://doi.org/10.1016/j.rser.2018.10.016>.
- [18] L. Yang, S. Wang, K. Blinn, M. Liu, Z. Liu, Z. Cheng, M. Liu. Enhanced Sulfur and Coking Tolerance of a Mixed Ion Conductor for SOFCs: $\text{BaZr}_{0.1}\text{Ce}_{0.7}\text{Y}_{0.2-x}\text{Yb}_x\text{O}_{3-\delta}$. *Science*. 2009, 326, 126-129. <https://doi.org/10.1126/science.1174811>
- [19] J. Wang, X. Xiao, Y. Liu, K. Pan, H. Pang, S. Wei. The application of CeO_2 -based materials in electrocatalysis. *J. Mater. Chem. A*, 2019, 7, 17675-17702. <https://doi.org/10.1039/C9TA04804A>.
- [20] A. Fuerte, R. X. Valenzuela, M. J. Escudero. Role of Dopants on Ceria-based Anodes for IT-SOFCs Powered by Hydrocarbon Fuels. *Uni. J. Electrical and Electronic Engineering*, 2017, 5(3), 45-55. <https://doi.org/10.13189/ujeee.2017.050301>
- [21] B. Bochentyn, P. Błaszczak, M. Gazda, A. Fuerte, S. -F. Wang, P. Jasiński. Investigation of praseodymium and samarium co-doped ceria as an anode catalyst for DIR-SOFC fueled by biogas. *Int. J. Hydrog. Energy*, 2020, 45(53), 29131-29142. <https://doi.org/10.1016/j.ijhydene.2020.07.146>.
- [22] C. Gaudillère, P. Vernoux, C. Mirodatos, G. Caboche, D. Farrusseng. Screening of ceria-based catalysts for internal methane reforming in low temperature SOFC. *Catal. Today*, 2010, 157(1-4), 263-269. <https://doi.org/10.1016/j.cattod.2010.02.062>.
- [23] D. E. P. Vanpoucke, P. Bultinck, S. Cottenier, V. V. Speybroeck. Isabel Van Driessche, Aliovalent doping of CeO_2 : DFT study of oxidation state and vacancy effects. *J. Mater. Chem. A*, 2014, 2, 13723-13737. <https://doi.org/10.1039/c4ta02449d>.
- [24] R. Jacot, R. Moré, R. Michalsky, A. Steinfeld, G. R. Patzke. Trends in the phase stability and thermochemical oxygen exchange of ceria doped with potentially tetravalent metals. *J. Mater. Chem. A*, 2017, 5, 19901-19913. <https://doi.org/10.1039/C7TA04063F>
- [25] S. A. Kumar, P. Kuppusami, S. Amirthapandian, Y. Fu. Effect of Sm co-doping on structural, mechanical and electrical properties of Gd doped ceria solid electrolytes for intermediate temperature solid oxide fuel cells. *Int. J. Hydrog. Energy*, 2020, 45(54), 29690-29704. <https://doi.org/10.1016/j.ijhydene.2019.10.098>.
- [26] C. B. Gopal, S. M. Haile. An electrical conductivity relaxation study of oxygen transport in samarium doped ceria. *J. Mater. Chem. A*, 2014, 2, 2405-2417. <https://doi.org/10.1039/C3TA13404K>
- [27] A. Kabir, M. Espineira-Cachaza, E. M. Fiordaliso, D. Ke, S. Grasso, B. Merle, V. Esposito. Effect of cold sintering process (CSP) on the electro-chemo-mechanical properties of Gd-doped ceria (GDC). *J. Eur. Ceram. Soc.*, 2020, 40(15), 5612-5618. <https://doi.org/10.1016/j.jeurceramsoc.2020.06.010>
- [28] T. Y. Yeo, J. Ashok, S. Kawi. Recent developments in sulphur-resilient catalytic systems for syngas production. *Renew. Sust. Energ. Rev.*, 2019, 100, 52-70. <https://doi.org/10.1016/j.rser.2018.10.016>.

- [29] W. Lai, S. M. Haile. Impedance Spectroscopy as a Tool for Chemical and Electrochemical Analysis of Mixed Conductors: A Case Study of Ceria. *J. Am. Ceram. Soc.*, 2005, 88(11), 2979–2997. <https://doi.org/10.1111/j.1551-2916.2005.00740.x>.
- [30] W. C. Chueh, Y. Hao, W. Jung, S. M. Haile. High electrochemical activity of the oxide phase in model ceria–Pt and ceria–Ni composite anodes. *Nat. Mater.*, 2011, 11(2), 155-161. <https://doi.org/10.1038/nmat3184>.
- [31] W. H. Kan, A. J. Samson, V. Thangadurai. Trends in electrode development for next generation solid oxide fuel cells, *J. Mater. Chem. A*, 2016, 4, 17913-17932. <https://doi.org/10.1039/C6TA06757C>.
- [31] E. D. Wachsman, K. T. Lee. Lowering the Temperature of Solid Oxide Fuel Cells. *Science*, 2011, 334, 935-939. <https://doi.org/10.1126/science.1204090>.
- [32] Chunwen Sun, Ulrich Stimming. Recent anode advances in solid oxide fuel cells. *J. Power Sources*, 2007, 171(2), 247-260. <https://doi.org/10.1016/j.jpowsour.2007.06.086>.
- [33] S. Cimino, G. Mancino, L. Lisi. Ethane catalytic partial oxidation to ethylene with sulphur and hydrogen addition over Rh and Pt honeycombs. *Catal. Today*, 2014, 228, 131-137. <https://doi.org/10.1016/j.cattod.2013.10.060>.
- [34] P. Boldrin, E. Ruiz-Trejo, J. Mermelstein, J. M. B. Menéndez, T. R. Reina, N. P. Brandon. Strategies for Carbon and Sulfur Tolerant Solid Oxide Fuel Cell Materials, Incorporating Lessons from Heterogeneous Catalysis. *Chem. Rev.*, 2016, 116(22), 13633-13684. <https://doi.org/10.1021/acs.chemrev.6b00284>.
- [35] H. He, R. J. Gorte, J. M. Vohs. Highly Sulfur Tolerant Cu-Ceria Anodes for SOFCs. *Electrochemical and Solid-State Letters*, 2005, 8(6), A279-A280. <https://doi.org/10.1149/1.1896469>
- [36] M. Gong, X. Liu, J. Tremblay, Christopher Johnson. Sulfur-tolerant anode materials for solid oxide fuel cell application. *J. Power Sources*, 2007, 168, 289-298. <https://doi.org/10.1016/j.jpowsour.2007.03.026>.
- [37] Z. Wang, W. Weng, K. Cheng, P. Du, G. Shen, G. Han. Catalytic modification of Ni–Sm-doped ceria anodes with copper for direct utilization of dry methane in low-temperature solid oxide fuel cells. *J. Power Sources*, 2008, 179, 541-546. <https://doi.org/10.1016/j.jpowsour.2008.01.040>.
- [38] Z. Liu, B. Liu, D. Ding, M. Liu, F. Chen, C. Xia. Fabrication and modification of solid oxide fuel cell anodes via wet impregnation/infiltration technique. *J. Power Sources*, 2013, 237, 243-259. <https://doi.org/10.1016/j.jpowsour.2013.03.025>.
- [39] S. P. Jiang, Nanoscale and nano-structured electrodes of solid oxide fuel cells by infiltration: Advances and challenges, *Int. J. Hydrog. Energy*, 2012, 37, 449-470. <https://doi.org/10.1016/j.ijhydene.2011.09.067>.
- [40] C. H. Bartholomew. Mechanisms of catalyst deactivation. *Appl. Catal. A: Gen.*, 2001, 212, 17-60. [https://doi.org/10.1016/S0926-860X\(00\)00843-7](https://doi.org/10.1016/S0926-860X(00)00843-7).
- [41] N. W. Kwak, S. J. Jeong, H. G. Seo, S. Lee, Y. Kim, J. K. Kim, P. Byeon, S. Chung, W. Jung. In situ synthesis of supported metal nanocatalysts through heterogeneous doping. *Nat. Commun.*, 2018, 9, 4829-4836. <https://doi.org/10.1038/s41467-018-07050-y>.
- [42] D. Neagu, T. Oh, D. N. Miller, Hervé Ménard, Syed M. Bukhari, Stephen R.

- Gamble, Raymond J. Gorte, John M. Vohs, John T. S. Irvine. Nano-socketed nickel particles with enhanced coking resistance grown in situ by redox exsolution. *Nat. Commun.*, 2015, 6, 8120-8129. <https://doi.org/10.1038/ncomms9120>.
- [43] L. Fan, B. Zhu, P. Su, Chuanxin He, Nanomaterials and technologies for low temperature solid oxide fuel cells: Recent advances, challenges and opportunities, *Nano Energy*, 2018, 45, 148-176. <https://doi.org/10.1016/j.nanoen.2017.12.044>.
- [44] A. M. Abdalla, S. Hossain, A. T. Azad, P. M. I. Petra, F. Begum, S. G. Eriksson, A. K. Azad, Nanomaterials for solid oxide fuel cells: A review, *Renew. Sust. Energ. Rev.*, 2018, 82(1), 353-368. <https://doi.org/10.1016/j.rser.2017.09.046>.
- [45] Z. Liu, D. Ding, M. Liu, X. Ding, D. Chen, X. Li, C. Xia, M. Liu, High-performance, ceria-based solid oxide fuel cells fabricated at low temperatures. *J. Power Sources*, 2013, 241, 454-459. <https://doi.org/10.1016/j.jpowsour.2013.04.130>.
- [46] M. Chlipała, P. Błaszczak, S.-F. Wang, P. Jasiński, B. Bochentyn. In situ study of a composition of outlet gases from biogas fuelled Solid Oxide Fuel Cell performed by the Fourier Transform Infrared Spectroscopy. *Int. J. Hydrog. Energy*, 2019, 44(26), 13864-13874. <https://doi.org/10.1016/j.ijhydene.2019.03.243>.
- [47] J. Jung, A. H. MacDonald. Magnetoelectric coupling in zigzag graphene nanoribbons. *Phys. Rev. B*, 2010, 81, 1954081-1954085. <https://doi.org/10.1103/PhysRevB.81.195408>.
- [48] G. Kresse, J. Furthuller. Efficient iterative schemes for *ab initio* total-energy calculations using a plane-wave basis set. *Phys. Rev. B*, 1996, 54(16), 11169-11186. <https://doi.org/10.1103/PhysRevB.54.11169>.
- [49] G. Kresse, D. Joubert. From ultrasoft pseudopotentials to the projector augmented-wave method. *Phys. Rev. B*, 1999, 59(3), 1758-1775. <https://doi.org/10.1103/PhysRevB.59.1758>.
- [50] D. Kim. Lattice Parameters, Ionic Conductivities, and Solubility Limits in Fluorite-Structure MO₂ Oxide [M = Hf⁴⁺, Zr⁴⁺, Ce⁴⁺, Th⁴⁺, U⁴⁺] Solid Solutions. *J. Am. Ceram. Soc.*, 1989, 72, 1415-1421. <https://doi.org/10.1111/j.1151-2916.1989.tb07663.x>.
- [51] R. D. Shannon. Revised effective ionic radii and systematic studies of interatomic distances in halides and chalcogenides. *Acta. Cryst.*, 1976, A32, 751-767. <https://doi.org/10.1107/S0567739476001551>.
- [52] S. Zeng, Y. Wang, S. Ding, J. J.H.B. Sattler, E. Borodina, L. Zhang, B. Weckhuysen, H. Su. Active sites over CuO/CeO₂ and inverse CeO₂/CuO catalysts for preferential CO oxidation. *J. Power Sources*, 2014, 256, 301-311. <https://doi.org/10.1016/j.jpowsour.2014.01.098>.
- [53] T. H. Etsell, S. N. Flengas. The Electrical Properties of Solid Oxide Electrolytes. *Chem. Rev.*, 1970, 70(3), 339-376. <https://doi.org/10.1021/cr60265a003>.
- [54] M. V. Twigg, M. S. Spencer. Deactivation of supported copper metal catalysts for hydrogenation reactions. *Appl. Catal. A: Gen.*, 2001, 212, 161-174. [https://doi.org/10.1016/S0926-860X\(00\)00854-1](https://doi.org/10.1016/S0926-860X(00)00854-1).
- [55] M. Boder, R. Dittmeyer. Catalytic modification of conventional SOFC anodes with a view to reducing their activity for direct internal reforming of natural gas. *J. Power Sources*, 2006, 155(1), 13-22. <https://doi.org/10.1016/j.jpowsour.2004.11.075>.

- [56] F. Zurloa, A. Iannaci, V. M. Sglavob, E. D. Bartolomeo. Copper-based electrodes for IT-SOFC. *J. Euro. Ceram. Soc.*, 2019, 39, 17-20. <https://doi.org/10.1016/j.jeurceramsoc.2018.02.029>.
- [57] W. Li, B. Guan, M. Liu, B. Wei, X. Zhu, Z. Wang, Z. Lü. On the limiting factor of impregnation methods for developing Cu/CeO₂ anodes for solid oxide fuel cells. *J. Solid State Electr.*, 2018, 22(6), 1735-1743. <https://doi.org/10.1007/s10008-017-3876-9>.
- [58] Y. Dong, S. Hampshire, J. Zhou, G. Meng. Synthesis and sintering of Gd-doped CeO₂ electrolytes with and without 1 at.% CuO doping for solid oxide fuel cell applications. *Int. J. Hydrog. Energy*, 2011, 36, 5054-5066. <https://doi.org/10.1016/j.ijhydene.2011.01.030>.
- [59] S. Jung, C. Lu, H. He, K. Ahn, R. J. Corte, J. M. Vohs. Influence of composition and Cu impregnation method on the performance of Cu/CeO₂/YSZ SOFC anodes. *J. Power Sources*, 2006, 154(1), 42-50. <https://doi.org/10.1016/j.jpowsour.2005.04.018>.
- [60] B. C. H. Steele, A. Heinzl. Materials for fuel-cell technologies. *Nature*, 2001, 414, 345-352. <https://doi.org/10.1038/35104620>.
- [61] W. Zając, L. Suescun, K. Świerczek, J. Molenda. Structural and electrical properties of grain boundaries in Ce_{0.85}Gd_{0.15}O_{1.925} solid electrolyte modified by addition of transition metal ions. *J. Power Sources*, 2009, 194, 2-9. <https://doi.org/10.1016/j.jpowsour.2008.12.020>.
- [62] D. K. Niakolas. Sulfur poisoning of Ni-based anode for Solid Oxide Fuel Cells in H/C-based fuels. *Appl. Catal. A: Gen.*, 2014, 486, 123-142. <https://doi.org/10.1016/j.apcata.2014.08.015>.
- [63] G. Postole, F. Bosselet, G. Bergeret, S. Prakash, P. Gélin. On the promoting effect of H₂S on the catalytic H₂ production over Gd-doped ceria from CH₄/H₂O mixtures for solid oxide fuel cell applications. *J. Catal.*, 2014, 316, 149-163. <https://doi.org/10.1016/j.jcat.2014.05.011>.
- [64] J. B. Wang, D. Tsai, T. Huang, Synergistic Catalysis of Carbon Monoxide Oxidation over Copper Oxide Supported on Samaria-Doped Ceria. *J. Catal.*, 2002, 208, 370-380. <https://doi.org/10.1006/jcat.2002.3580>.
- [65] S. Poulston, P. M. Parlett, P. Stone, M. Bowker. Surface oxidation and reduction of CuO and Cu₂O studies using XPS and XAES. *Sur. interface anal.*, 1996, 14, 811-820. [https://doi.org/10.1002/\(SICI\)1096-9918\(199611\)24:12<811::AID-SIA191>3.0.CO;2-Z](https://doi.org/10.1002/(SICI)1096-9918(199611)24:12<811::AID-SIA191>3.0.CO;2-Z).
- [66] T. Montini, M. Melchionna, M. Monai, P. Fornasiero. Fundamentals and Catalytic Applications of CeO₂-Based Materials. *Chem. Rev.*, 2016, 116, 5987-6041. <https://doi.org/10.1021/acs.chemrev.5b00603>.
- [67] M. A. Ocsachoque, J. I. E. Russman, B. Irigoyen, D. Gazzoli, M. G. González. Experimental and theoretical study about sulfur deactivation of Ni/CeO₂ and Rh/CeO₂ catalysts. *Mater. Chem. Phys.*, 2016, 172, 69-76. <https://doi.org/10.1016/j.matchemphys.2015.12.062>.
- [68] National Energy Administration. Natural gas: GB 17820-2018. Beijing: Standards Press of China, 2018.

[69] International Organization for Standardization/Natural Gas Technical Committee (ISO/TC193). Natural gas - Quality designation: ISO 13686:2013. Geneva: ISO, 2013.

[70] German Institute for Standardisation. Gas infrastructure – Quality of gas – Group H: DIN EN 16726 2016-04. Frankfurt am Main: German Institute for Standardisation, 2016.

[71] American Gas Association. Natural Gas Contract Measurement and Quality Clauses (Q0904): AGA REPORT 4A-2009. Washington DC: American Gas Association, 2009.

[72] C. Duan, R. J. Kee, H. Zhu, C. Karakaya, Y. Chen, S. Ricote, A. Jarry, E. J. Crumlin, D. Hook, R. Braun, N. P. Sullivan, R. O’Hayre. Highly durable, coking and sulfur tolerant, fuel-flexible protonic ceramic fuel cells. *Nature*, 2018, 557,217-222. <https://doi.org/10.1038/s41586-018-0082-6>.

Declaration of Competing Interest

The authors declare that they have no known competing financial interests or personal relationships that could have appeared to influence the work reported in this paper.

Highlights

- A (Cu, Sm)CeO₂ anode with anchored Cu nanoparticles was fabricated
- The Cu nanoparticles particle size ranges from 20 to 50 nm
- The prepared cell exhibits a good performance with dry methane as fuel
- Such an anode shows good resistance to coking and sulfur poisoning
- The single SOFC shows good stability with natural gas as fuel